Hindawi
Advances in Materials Science and Engineering
Volume 2023, Article ID 9829015, 1 page
https://doi.org/10.1155/2023/9829015

Retraction

Retracted: Processing and Properties of AlCoCrFeNi High Entropy Alloys: A Review

Advances in Materials Science and Engineering

Received 26 December 2023; Accepted 26 December 2023; Published 29 December 2023

This article has been retracted by Hindawi, as publisher, following an investigation undertaken by the publisher [1]. This investigation has uncovered evidence of systematic manipulation of the publication and peer-review process. We cannot, therefore, vouch for the reliability or integrity of this article.

Please note that this notice is intended solely to alert readers that the peer-review process of this article has been compromised.

Wiley and Hindawi regret that the usual quality checks did not identify these issues before publication and have since put additional measures in place to safeguard research integrity.

We wish to credit our Research Integrity and Research Publishing teams and anonymous and named external researchers and research integrity experts for contributing to this investigation.

The corresponding author, as the representative of all authors, has been given the opportunity to register their agreement or disagreement to this retraction. We have kept a record of any response received.

References

[1] P. Gopal, K. Soorya Prakash, V. Kavimani, and G. Rajendiran, "Processing and Properties of AlCoCrFeNi High Entropy Alloys: A Review," *Advances in Materials Science and Engineering*, vol. 2022, Article ID 1190161, 13 pages, 2022.

Hindawi
Advances in Materials Science and Engineering
Volume 2022, Article ID 1190161, 13 pages
https://doi.org/10.1155/2022/1190161

Review Article

Processing and Properties of AlCoCrFeNi High Entropy Alloys: A Review

P.M. Gopal,[1] **K. Soorya Prakash**,[2] **V. Kavimani**,[1] **and Gopal Rajendiran**[3]

[1]*Centre for Material Science, Mechanical Engineering, Karpagam Academy of Higher Education, Coimbatore 641021, Tamil Nadu, India*
[2]*Department of Mechanical Engineering, Anna University Regional Campus Coimbatore, Coimbatore 641046, Tamil Nadu, India*
[3]*Department of Motor Vehicle Engineering, Defence University College of Engineering, Bishoftu, Ethiopia*

Correspondence should be addressed to Gopal Rajendiran; rajendiran.gopal@dec.edu.et

Received 19 May 2022; Accepted 1 September 2022; Published 3 October 2022

Academic Editor: K. Raja

The aim of this study is to carry out a focused literature review on the mechanical and tribological behaviour of AlCoCrFeNi High Entropy Alloys (HEA). HEAs are a proficient class of alloys designed by the use of several constituent alloying elements in equiatomic or close to equiatomic ratios. In view of their distinctive property range, there has been huge attention on this class of alloys. Among the various group of HEAs, AlCoCrFeNi-based HEAs have attracted interest due to their enhanced properties. Various AlCoCrFeNi-based HEAs are developed by adding additional elements such as Mo, Ti, and Zr. The effect of these alloying constituents on the mechanical, metallurgical, and tribological performance of the AlCoCrFeNi HEA is discussed in detail. In addition to that, the various techniques used to produce these HEAs are also discussed.

1. Introduction

Human civilisation is differed and described mainly based on the materials such as that of the Stone Age, Bronze Age, and Steel Age. Development of newer materials takes society to the next level such as alloys, superalloys, and composites. Conventionally the newer materials are developed by adding two or more materials together in which a base material has a higher proportion while other elements are added in minor levels. When a metal is mixed with a minor amount of different metals it is called as alloy and the composites are made by mixing ceramics or fibres with a base material altogether for improving properties. In contrast to all these materials designs, multiple materials are mixed together in equal proportions to get the high-performance material that are new age materials called as High Entropy Alloys. HEAs named by Yeh et al. [1] contain multiple elements mixed together mostly at an equal proportion that abstain from the "Base Element" conception. Its name is owing to the high mixing entropy of the indiscriminate mixing of elements and HEAs are currently being studied more [1–6]. However, researches on this alloy system are in the preliminary stage when compared to conventional alloys [7].

Preferably, HEAs are stated as alloys with a minimum of five primary elements, each of which has an atomic proportion between 5 and 35 percent [1]. The HEAs are prepared by mixing elements in equiatomic levels and also in non-equiatomic concentrations. Generally, HEAs with equiatomic concentrations possess high mixing entropy than the nonequiatomic alloys. Various HEAs were prepared mainly by using elements such as Al, Fe, Cr, Ni, Cu, Co, Si, Ti, Mo, Mn, Zr, and Zn. HEAs exhibit unusual properties that are far away from conventional alloy properties. For example, the hardness of the MoTiVFeNiZrCoCr HEA is more than 800HV and the hardness of the commonly known conventional hard material 316 stainless steel is below 200HV. A specific strength of the HEAs is also higher than that of aluminium, titanium, nickel, and iron-based alloys [3].

Among the various HEAs developed, AlCoCrFeNi and its allied HEAs are investigated in large numbers. The

equiatomic AlCoCrFeNi has enhanced strength (fracture strength 3531 MPa) and upright plasticity (compression strain 24.5%) [8]. A number of new HEAs are developed by varying one or more elements in the AlCoCrFeNi composition or by adding other elements with it. Generally, Ti, Zr, and Si are added in smaller proportions with this HEA system, and their influence on microstructure, phase transformation, and mechanical characteristics was examined.

A basic study on AlCoCrFeNi HEA revealed that the BCC structured solid solution with a refined microstructure of 20 nm in grain size could be attained after 30 h milling. The stability in phase for the as-milled HEA powder is found good up to 500 C and a further increase in temperature has resulted in FCC structure. The coexistence of BCC and FCC phases was found in the HEA after spark plasma sintering (SPS) consolidation at 900 C. It exhibits superior characteristics like 625 HV microhardness and compressive strength of 1907 Mpa. The HEA obtained by SPS (Applied Temperature and Pressure of 900 C and 50 Mpa for 10 min in argon atmosphere) of 60 h milled CoCrFeNiAl powder shows a relative density of more than 99%. And the developed material exhibited more hardness than many commercially used hard-facing alloys (e.g. Stellite, around 500 HV) [9]. So, the current study attempts to review the effect of additional elements on the mechanical, corrosion, and wear properties of the AlCoCrFeNi HEAs.

2. Processing Methodologies of AlCoCrFeNi-Based HEAs

Generally, HEA developing methodologies can be divided depending on the initial state of the alloy preparation. In general, mechanical alloying then isostatic pressing, arc melting, laser cladding, and surface coating (plasma spray and LASER) are universally utilised for HEA development. Some other advanced methods for AlCoCrFeNi-based HEA preparation such as electrochemical techniques are also evolving [3].

2.1. Arc Melting. Arc melting is a prominent liquid state method in which the HEAs are attained through melting several components (minimum of 5 times) in the arc melting furnace. The alloy remelting is done for homogeneity and the general arrangement of the arc melting method is shown in (Figure 1). A very high torch temperature range of above 3000 C can be attained in the arc melting furnace and by varying the electrical power, the temperature can be managed. Thus, the majority of high melting point elements can be assorted through this liquid state processing [11].

The AlCoCrFeNi ingots formed by arc melting of 99.9% pure elements on copper crucible having water-cooling capability under pure argon environment exhibit BCC phase which is identified through XRD analysis [12]. The yield strength, fracture strength, and plastic strain of 1320 MPa, 2670 MPa, and 22.5% are obtained for AlCoCrFeNi HEA developed through arc melting.

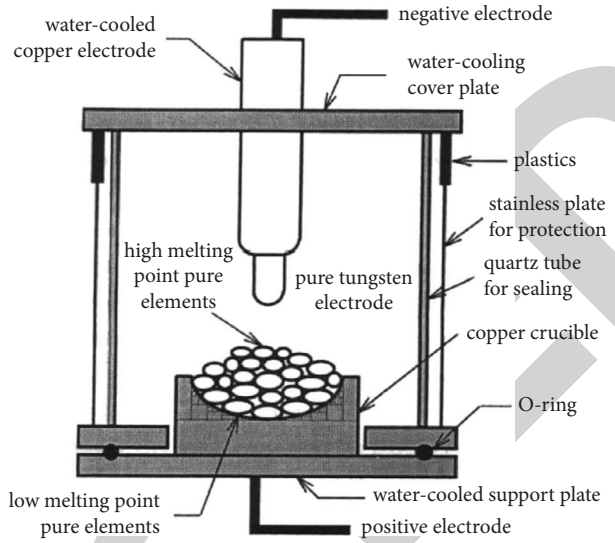

Figure 1: Schematic representation of arc melting process [10].

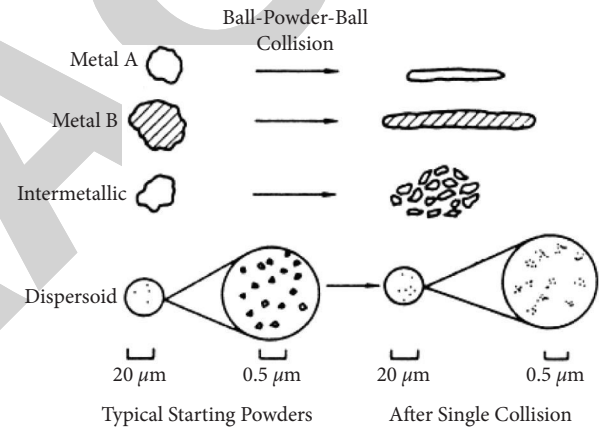

Figure 2: Mechanism of mechanical alloying [14].

2.2. Mechanical Alloying. It is a simple method of solid-state powder processing that comprises repetitive cold welding, fracturing, and rewelding of particles with the help of high-energy ball milling [13]. The mechanism of mechanical alloying is given in (Figure 2). It has been reported as it has the ability to develop diverse equilibrium and nonequilibrium alloys initiated with mixed elemental or prealloyed powders [15]. This method is not similar to the metal powder processing methodology in which metal powders are mixed to produce superalloys.

HEAs developed through mechanical alloying and consolidation possess higher pore density than that of HEAs made up by casting. On contrary, the melting method directs to segregation issues, whereas consistent chemical dispersion and solid solubility extension can be attained by the mechanical alloying process [15]. Additionally, it is a potential technique that can simply be exploited to develop superior property nanocrystalline materials.

Al, Co, Cr, Fe, and Ni powders of ≤ 60 μm size and 99.7% purity were mechanically alloyed in equiatomic compositions [16]. The planetary ball mill rotating at 300 rpm is used

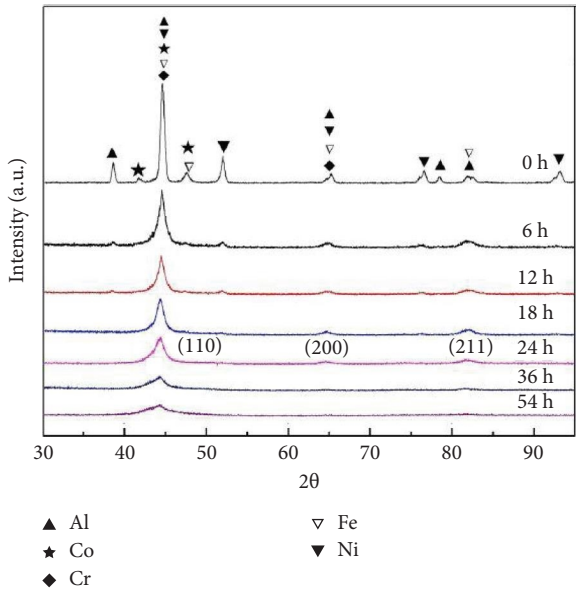

Figure 3: XRD patterns of AlCoNiCrFe HEA with respect to milling time [16].

to mix the powders with the ball-to-powder ratio of 15:1. Ball material used is chrome steel and the process regulating agent used to avert unwanted reactions such as cold welding and oxidisation is toluene. The alloying process is tracked by extracting the powders from the ball mill every 6 h. For consolidation, the powders are then sintered after 60 h of alloying. Then extracted powders are analysed through an X-ray diffractometer in order to identify the alloy formation and the results were shown in (Figure 3). A remarkable decrease in intensity of the mixed elements was identified after milling for 6 h and the peaks are getting broader and some peaks become unseen. This phenomenon is credited to good crystal size and hefty lattice strain [17, 18]. Only three main intensive peaks with BCC structure ((110), (200), and (211)) are visible after 24 h milling which shows the establishment of a single solid solution (AlCoNiCrFe HEA). Furthermore, it was identified that there is no significant change in peaks for further milling. The calculated lattice parameter for the HEA powder milled for 24 h is 2.878 Å and it is coinciding with reports described by Zhang et al. [19]. Additionally, the HEA powders obtained after 60 h has a grain size of 15 nm after eliminating the instrumental and strain contributions, which is in fine conformity with the value described by Ji et al. [17].

2.3. Plasma Spray Process. It is a liquid state processing technique particularly used to formulate HEA coatings. The HEA coating over the specific surface is achieved through high-velocity plasma spraying, which furnishes an even defensive deposit [18]. This procedure involves melting of HEA powders on the arranged surfaces for spray deposition as shown in (Figure 4). The necessary temperature for melting is obtained from the thermal spraying gun by combusting gases through electric arcs. Since the objective material is heated up gradually, it is transformed into a molten state and the acceleration of the material will be done through compressed gas. This controlled particle stream will pass to the target and be allowed to hit the target face and thin flat platelets were formed. The formed platelets are well-suited to the prepared surface irregularities. Furthermore, these sprayed particles are mounted up to form coatings on the target by cooling and building up one after another into an organised form.

The AlCoCrFeNi powder that is mechanically alloyed for 10 hours exhibits BCC as the major phase and a minor FCC phase is also detected. But the coated HEA which undergoes the high-temperature atmosphere during the plasma spray process exhibits the FCC phase. A typical lamellar thermal spray coating microstructure was observed [21]. The developed layer structure is suffered from a number of voids which can be stated as pores and interlamellar cracks. The coating exhibits 4.13 GPa Vickers microhardness.

2.4. Laser Cladding. This procedure comprises quick heating and cooling, more uniform and dense cladding, and less microscopic flaws as its advantages. Furthermore, it is simply attained and minimal thermal effect on the target material, and a small dilution rate is observed [22]. The laser cladding method is comparable to the plasma spray process technique in that it has an energy resource to melt the feedstock that is being applied to the target surface. The difference is it has intense LASER as heat origin, and it melts the substrate that the feedstock is being applied to as revealed in (Figure 5). Greater bond strength is achieved than the plasma spray procedure since this method usually fallouts in a metallurgical bond. The major advantage of this technique is the size of heat affected region which is shallow. This can be attributed to the ability of the laser beam to be concentrated on a narrow region or point. This characteristic results in minimised cracking, distortion, or modification in the substrate's metallurgy. In addition, the dilution of the coating with materials from the substrate is minimal because of the lower total heat [24].

The mechanically mixed powders of Ni, Co, Fe, Cr, Al, and Cu, with Si, were preloaded on a 2 mm thick AZ31 magnesium strip, and a LASER is passed over to produce the HEA layer [25]. The HEA clads exhibit primary BCC phase and traces of FCC. The developed surface exhibits better hardness and corrosion resistance. The hardness of the developed HEA clad surface is 10 times higher than the base alloy and the corrosion densities of the developed surface are lower than the base alloy surface under 3.5% NaCl solution.

3. Effect of Alloying Elements on AlCoCrFeNi HEAs

Along with AlCoCrFeNi HEA, some of the alloying elements have been added to improve their properties. A detailed review of the impact of various alloying elements on AlCoCrFeNi's properties is presented in this section. The effect of alloying elements such as Mo, Zr, B, Si, Nb, V, Fe, and Ti on microstructure and mechanical characteristics of AlCoCrFeNi are discussed in detail.

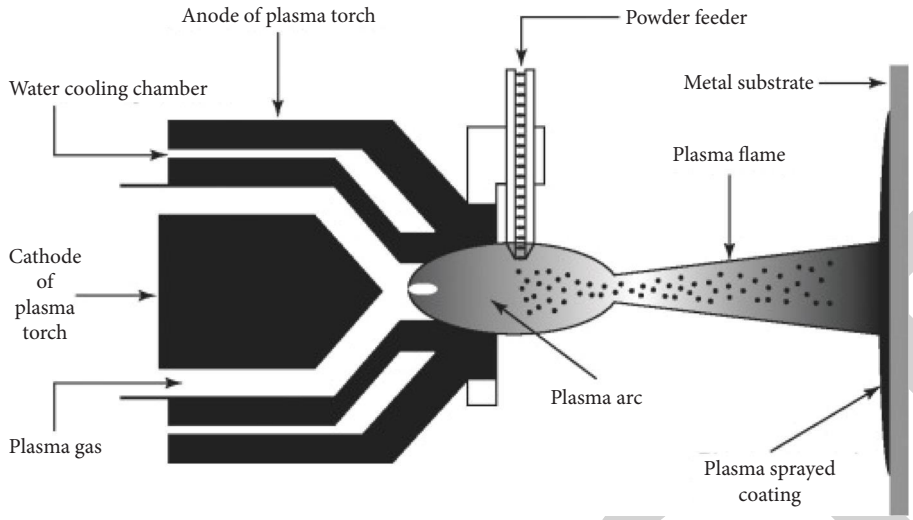

Figure 4: Plasma spray technique [20].

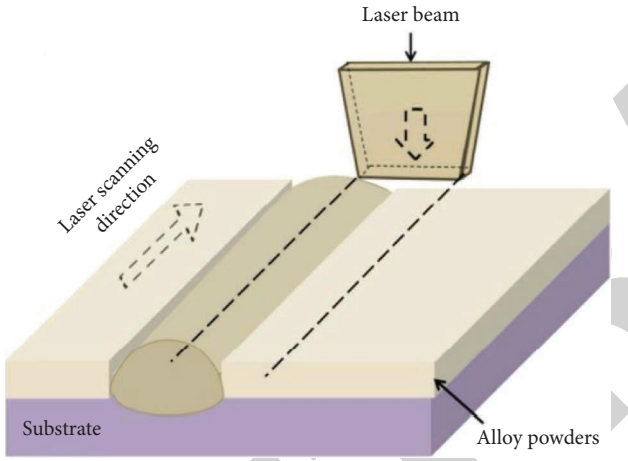

Figure 5: Laser cladding [23].

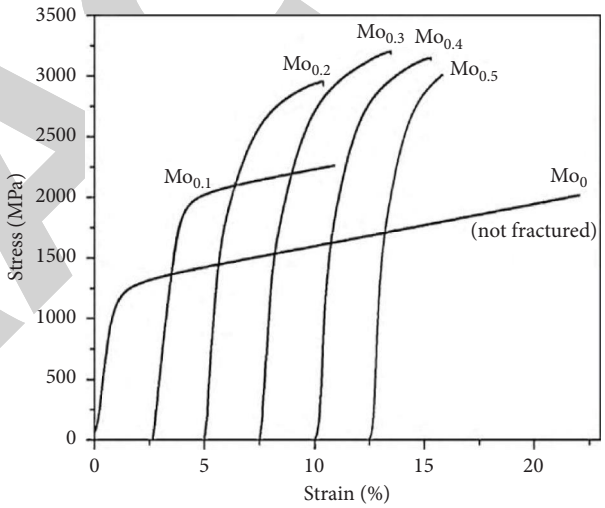

Figure 6: Stress–strain curves of as-cast $AlCoCrFeNiMo_x$ ($x = 0$ to 0.5) HEA [26].

3.1. Effect of Molybdenum. $AlCoCrFeNiMo_x$ ($x = 0$, 0.1, 0.2, 0.3, 0.4, and 0.5 in molar ratio) multicomponent alloys were fabricated through the arc melting method, and noteworthy variations in the structure and characteristics of AlCoCrFeNi alloy was identified as a result of Mo addition [26]. $Mo_{0.1}$ alloy shows a single BCC solid solution structure that is similar to Mo_0 alloy, i.e., AlCoCrFeNi. The alloy exhibited a classical laminar eutectic structure when Mo quantity increased further (> 0.1). Obviously, the strength of the alloy was improved; at the same time, the loss of ductility takes place. The maximum yield strength is attained at $x = 0.5$ (2757 MPa), and the maximum compressive fracture strength is reached at $x = 0.3$ (3208 MPa) and the same is shown in the compressive stress–strain curve shown in Figure 6.

3.2. Effect of Zirconium. Two kinds of microstructures were observed for $AlCoCrFeNiZr_x$ ($x = 0$, 0.008, 0.1, 0.3, and 0.5) alloys produced through the arc melting method. One is a periodic structure due to spinodal decomposition that consists of ordered BCC and BCC solid solution phase and the second one is a combination of the ordered BCC and Laves phase which alternatively nucleate and grow [12].

Even a low amount of Zr introduction can considerably enhance the properties when it goes under a compression test. The maximum yield strength of 1560 Mpa, the fracture strength of 3513 Mpa, and plastic strain of 29.5% are achieved for $AlCoCrFeNiZr_{0.008}$ alloy which are increased by 240 Mpa, 843 Mpa, and 7% than the base alloy, respectively. But the addition of Zr over 0.1 results in a significant decrease in fracture strength and plastic strain whereas the yield strength of the alloys surges with the increase in Zr quantity. And the impact of zirconium quantity on the properties of AlCoCrFeNi HEA is given in (Figures 7–10).

3.3. Effect of Boron. FCC phase structure with boride precipitation is obtained when the Boron addition is varied from $x = 0$ to $x = 1.0$ in $CuCoNiCrAl_{0.5}FeB_x$ (denoted as B-0

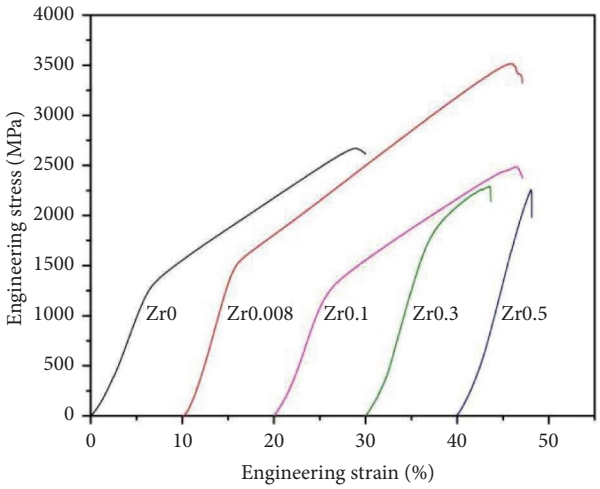

Figure 7: Stress–strain curves of $AlCoCrFeNiZr_x$ alloys (compressive) [12].

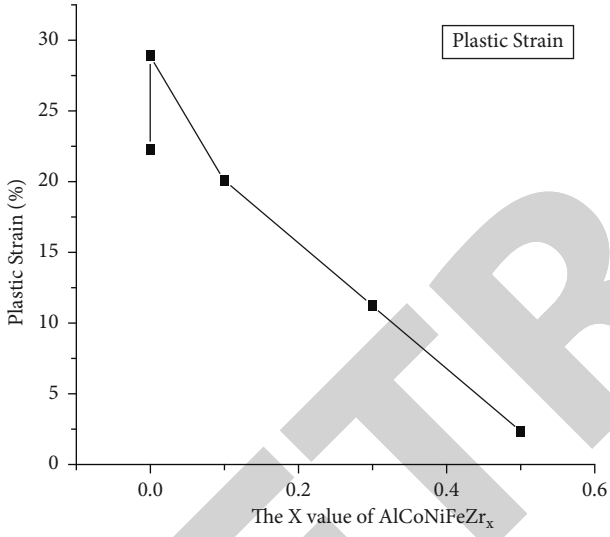

Figure 8: Impact of Zr on plastic strain for $AlCoCrFeNiZr_x$ HEAs [12].

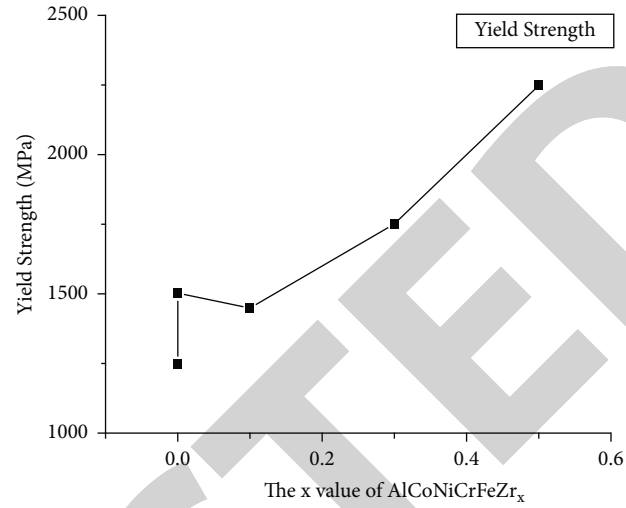

Figure 9: Effect of Zr content on yield strength for the $AlCoCrFeNiZr_x$ HEAs [12].

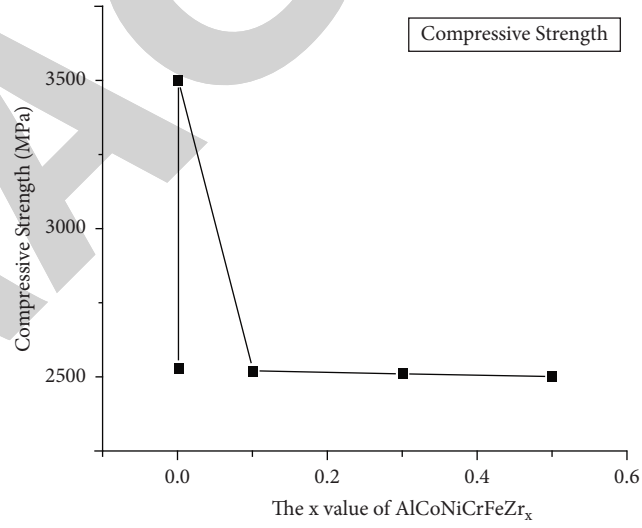

Figure 10: Influence of Zr content on compressive strength for the $AlCoCrFeNiZr_x$ HEAs [12].

to B-1.0 alloys) alloys [27]. The addition of boron increases the boride volume fraction in the alloy and their corresponding hardness values are enhanced from HV 232 to HV 736. The formation of boride enhances the value of high-temperature compression strength. The HEA through boride is less tough, i.e., the hardness of $CuCoNiCrAl_{0.5}FeB_x$ HEA based on boron content grows at the cost of toughness.

The increase in the amount of boron addition in $CuCoNiCrAl_{0.5}Fe$ HEA gives better high-temperature compression strength. The compression yield stress obtained at different temperatures that varied from room temperature to 1100 C for the $CuCoNiCrAl_{0.5}Fe$ HEA is shown in (Figure 11). A drastic increase in yield stress is exhibited by B-0.6 and B-1.0 HEA up to 300°C, B-0.2 HEA at 500°C, and B-0 HEA at 700°C. This promising temperature outcome for yield stress is associated with that persisting in superalloys. [28] The yield stress of the HEAs comprising boron is superior for higher boron content. Furthermore, it was identified that the boride addition plays a crucial role in promising temperature effects in view of the fact that the peak-strength temperature varies in the course of boron content. The rule of borides on the yield stress of developed HEAs is weakening at temperatures more than 900°C. All the HEAs irrespective of boron addition exhibit similar yield stress values above 900°C. So, it is vital to state that the mechanical characteristics of these modern HEAs could be regulated in a vast array by boron inclusion. The hardness and strengths at room temperature equal to Ti, Zr, or Pd-based bulk amorphous alloys can be attained by HEAs by boron addition [29]. In addition, it does not undergo glass transition and crystallisation as amorphous alloys at a glass transition temperature (T_g) and crystallisation temperature (T_x), respectively. They expose superior strength at high temperatures up to 700°C to 800°C as a result of their promising temperature effect.

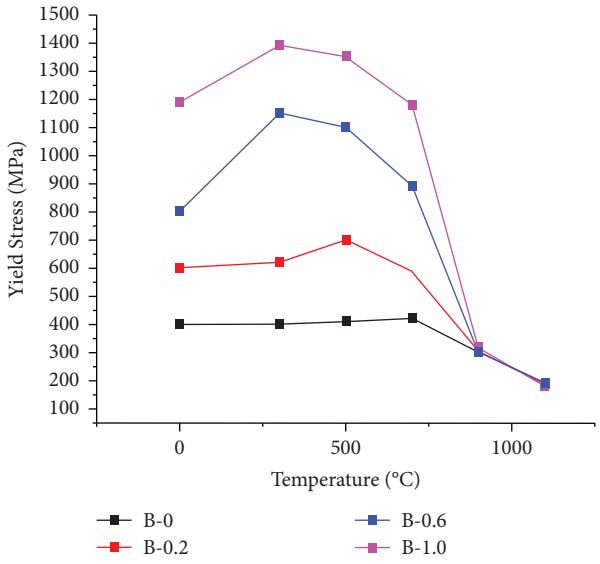

Figure 11: Requirement of yield stress on temperature for $CuCoNiCrAl_{0.5}Fe$. HEA with different boron contents [27].

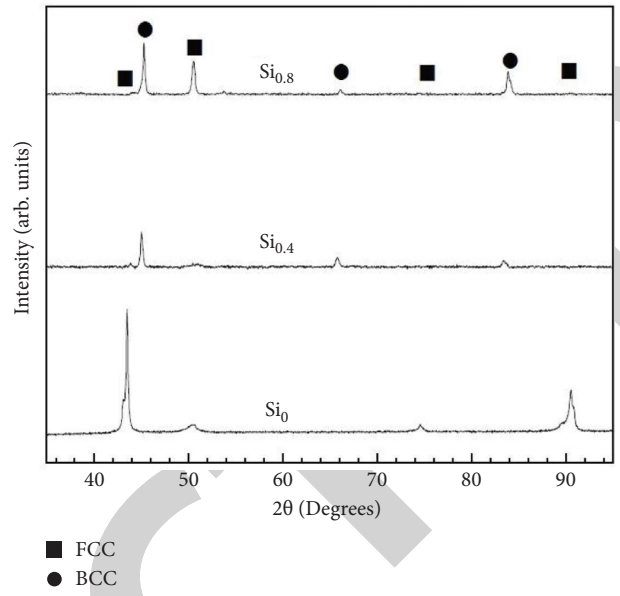

Figure 12: XRD pattern of the $Al_{0.5}CoCrCuFeNiSi_x$ (as-cast) [30].

3.4. Effect of Silicon. The peaks related to BCC structure begin to appear and their intensity upsurges with an increase in Si content. The XRD results publicised in Figure 12 show that the BCC peaks were shifted slightly towards the right with an increase in Si content being a sign of a decrease in the lattice parameter of the BCC phase. The calculated lattice constants of the BCC phases in the HEA show that the lattice constants are 2.867 Å and 2.859 Å for the HEA with Si = 0.4 and Si = 0.8, correspondingly. As the Si concentration rose, the crystal structure transitioned from FCC to BCC and also the lattice constant of the BCC phase changes [30].

The hardness of the $Al_{0.5}CoCrCuFeNiSi_x$ HEA increases with respect to Si concentration. The hardness of $Al_{0.5}CoCrCuFeNiSi_x$ improved when the content of silicon is differed from 0 to 0.8 and it is noteworthy that the hardness of the alloy having Si = 0.8 (653 HV) is 2.48 times higher when compared to the alloy without Si (263 HV).

3.5. Effect of Vanadium. The microstructure effects of $Al_{0.5}CoCrCuFeNiV_x$ ($x = 0$ to 2.0 in molar ratio) HEA shows that the alloys are consists of a simple FCC solid solution structure with small vanadium addition [31]. BCC structure becomes noticeable with spinodal decomposition and surrounds the FCC dendrites when the vanadium content is extended to 0.4. The volume fraction of the BCC structure phase upsurges as the vanadium concentration increases from $x = 0.4$ to 1.0. FCC dendrites are entirely replaced by BCC dendrites when $x = 1.0$. From $x = 0.6$ to 1.0, needle-like σ-phase forms, and BCC spinodal structure increases but it vanishes when $x = 1.2$ to 2.0.

When the amount of vanadium raised from 0.4 to 1.0, the hardness values of the HEA amplified and attains the peak value of 640 HV at $x = 1.0$ as shown in (Figure 13). Compared with the $Al_{0.5}CoCrCuFeNi$ HEA, the addition of vanadium upholds the HEA characteristics.

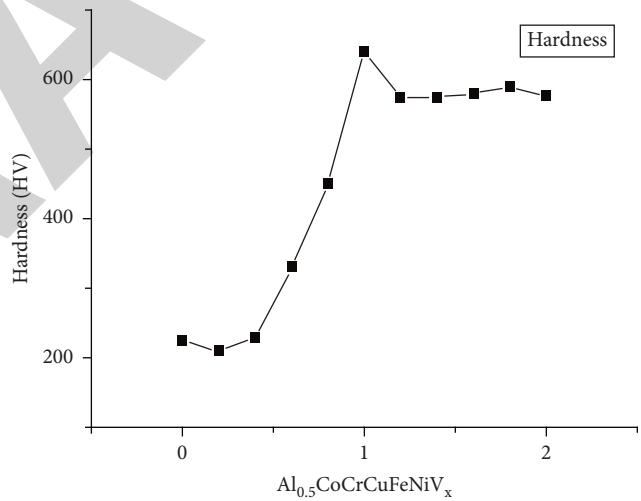

Figure 13: Hardness of $Al_{0.5}CoCrCuFeNiV_x$ HEA with different vanadium contents [31].

3.6. Effect of Niobium. $AlCoCrFeNb_xNi$ HEAs exhibit two phases that are BCC solid solution phase and the (CoCr) Nb type Laves phase. The HEA series shows the varying microstructures from hypoeutectic to hypereutectic and the Vickers hardness and compressive yield strength are almost in linear increment with the increase in Nb content [8].

From Figure 14 and Table 1, it can be noted that there is an extensive increase in yield strength from 1373 MPa to 2473 MPa with Nb addition whereas about 24.5% to 4.1% decreases in plastic strain limits are obtained. The linear increase in Vickers hardness of the developed HEA series is expressed as an equation i.e., $Y_{HV} = 454_x + 530$, where x and Y_{HV} denote the Nb content and Vickers hardness, respectively, and the same is shown in (Figure 15).

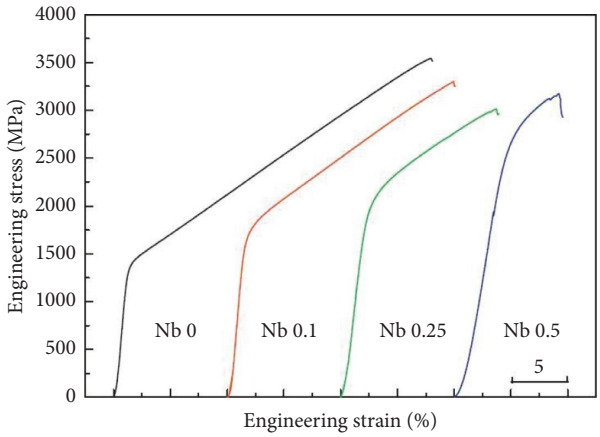

Figure 14: The compressive stress–strain curves of the AlCoCrFeNb$_x$Ni HEA ($x = 0$, 0.1, 0.25, and 0.5) [8].

Table 1: Mechanical properties of AlCoCrFeNb$_x$Ni ($x = 0$, 0.1, 0.25, and 0.5) alloy [8].

x	$\sigma_{0.2}$ (MPa)	σ_{max} (Mpa)	ε_p (%)	HV
0	1373	3531	24.5	520 ± 11
0.1	1641	3285	17.2	569 ± 11
0.25	1959	3008	10.5	668 ± 12
0.5	2473	3170	4.1	747 ± 10

$\sigma_{0.2}$, yield strength; σ_{max}, fracture strength; ε_p, plastic strain limits; HV, Vickers hardness.

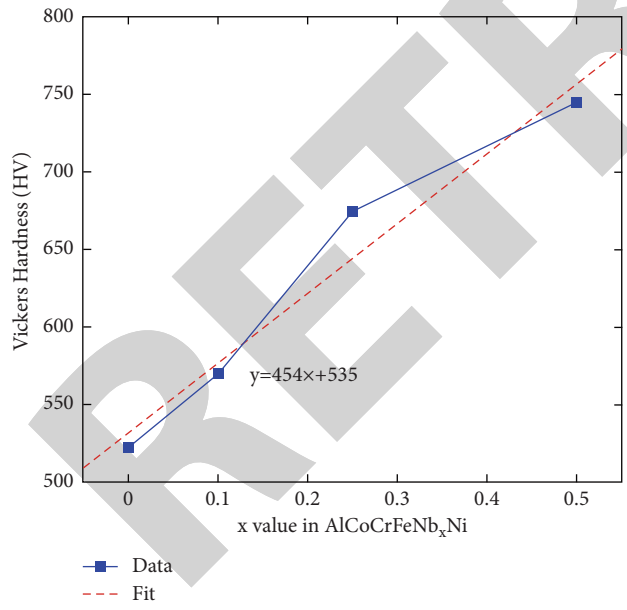

Figure 15: The hardness of AlCoCrFeNb$_x$Ni with respect to Nb. Contents ($x = 0$, 0.1, 0.25, and 0.5) [8].

3.7. Effect of Iron. A new HEA system, AlCoCrFeMoNi is designed with Mo to enhance the strength and thermal stability. The interrelation between the microstructural changes and hardness behaviour of AlCoCrFe$_x$Mo$_{0.5}$Ni HEA with the consequence of iron concentration is analysed [32]. The microstructure transforms to "polygrain" for Fe1.5 and

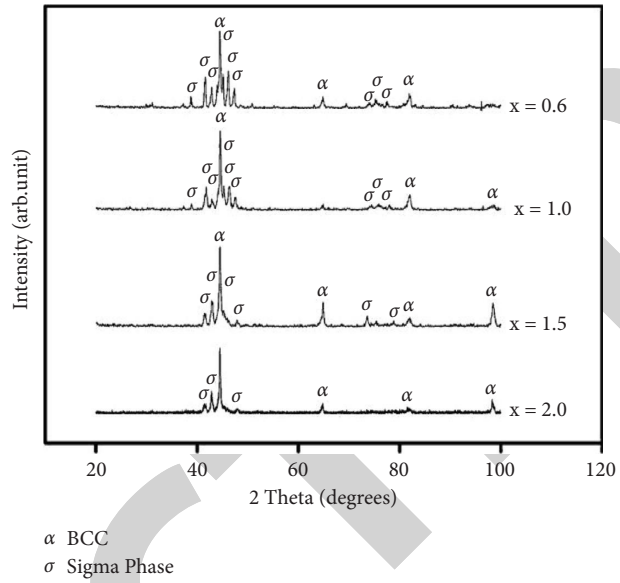

Figure 16: XRD of AlCoCrFexMo$_{0.5}$Ni HEA with different Fe contents [32].

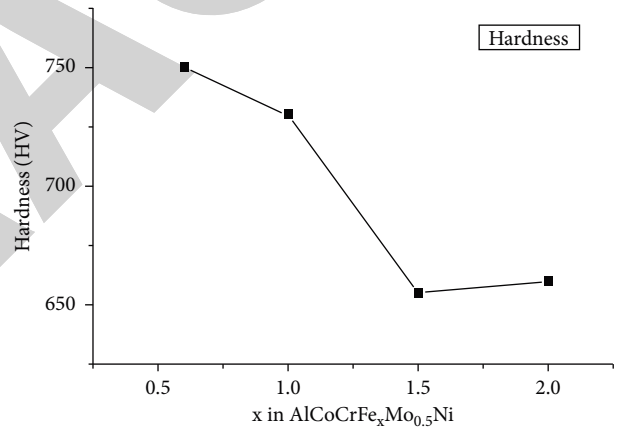

Figure 17: Vickers hardness of AlCoCrFexMo$_{0.5}$ Ni alloys with respect to Fe content [32].

Fe2.0 HEA from "dendritic" for Fe0.6 and Fe1.0 HEA with the increase in Fe content. The crystal structure of AlCoCrFe$_x$Mo$_{0.5}$Ni is a duplex structure having BCC solid solution and σ phase. But the increase in peak intensity of the BCC phase is higher than the σ phase with an increase in the volume fraction of iron content showing the decrement in the σ phase as evidenced by the XRD patterns given in (Figure 16).

Hardness increases with the addition of Mo in the system owing to the development of the hard σ phase and hardness raises from HV 356 to HV 730. Besides, with an HV of nearby 725, Fe0.6 and Fe1.0 HEA are around HV 100 harder than Fe1.5 and Fe2.0 HEA. This hardness drops off with a rise in the Fe content due to the corresponding decrease in the σ phase amount because of the soft nature of the BCC phase when related to the σ phase. The hardness values are measured in dendrites (with less σ phase) and interdendrites (with more σ phase) of the Fe0.6 HEA were HV643 and

Table 2: Overall hardness and microhardness (HV) of each phase in the four HEAs [33].

Al00Ti05	Al02Ti05	Al00Ti10			Al02Ti10			
Overall	Overall	Overall	ID	DR	Overall	ID (al - rich region)	ID (coarse η)	DR
509 ± 11	487 ± 5	654 ± 7	924 ± 33	617 ± 13	717 ± 13	1197 ± 110	910 ± 24	619 ± 12

HV898, individually. The influence of Fe concentration on the microhardness of the HEA is clearly shown in (Figure 17).

3.8. Effect of Aluminium and Titanium. The HEAs with lower Ti addition (0.05) possess lower hardness values owing to their primary FCC gamma phase. Slightly increased hardness was exhibited by $Al_{00}Ti_{05}$ as a result of η precipitates at the grain boundaries [33]. HEA hardness value increases significantly as the Ti content increased further (0.1) as shown in (Table 2). $Al_{00}Ti_{10}$ HEA exhibits 650 HV as its overall hardness which is higher than that of the HEAs with minor Ti addition (i.e., $Al_{00}Ti_{05}$ and $Al_{02}Ti_{05}$). This increase in hardness is credited to the development of the η phase in the interdendritic region of $Al_{00}Ti_{10}$ where the microhardness is around HV 900. Even though the interdendritic region of $Al_{02}Ti_{10}$ HEA has less amount of coarse η phases than that of $Al_{00}Ti_{10}$, the Widmanstatten structured needle-like η phase offers even superior hardness of up to HV 1200 which makes $Al_{02}Ti_{10}$ as the harder HEA (HV 717) among them.

4. Effect of Alloying Elements on Wear Properties

Wear is one of the important functional properties of materials. It is an erosion and displacement phenomenon of material from its original position on the surface performed by the activity of another surface. AlCoCrFeNi HEAs are reported as materials having greater wear resistance capability than the other metallic systems and alloys. Literature that discussed the influence of Fe, B, V, Al, and Ti-like alloying elements on the wear behaviour of AlCoCrFeNi HEAs is discussed in this section.

4.1. Effect of Iron. The wear behaviour of $AlCoCrFe_xMo_{0.5}Ni$ alloys with iron addition is explained with respect to the microstructural change and it is shown in (Figure 18). The $Fe_{0.6}$ and $Fe_{1.0}$ alloys exhibit dendritic structure, whereas it changes to polygrain for $Fe_{1.5}$ and $Fe_{2.0}$ HEAs. Primarily the alloy possesses BCC and σ phase, but with increases in the iron content, the vol. fraction of the BCC phase surges. Consequently, the wear resistance of the alloy decreases with increases in iron content [32]. However, $Fe_{2.0}$ shows signs of very poor wear resistance to $Fe_{1.5}$ which is not consistent with the hardness change.

The worn-out surfaces and wear debris of the $AlCoCrFe_xMo_{0.5}Ni$ alloys tested at different testing conditions are shown in Figure 19. The worn surfaces of the alloys expose their microstructural difference with abrasive scratches. Since the interdendrites are harder than the dendrites due to more σ phase the protrusion of the harder σ phase above the BCC phase is identified in the HEAs microstructure. Analysis of worn surface shows the presence of Oxygen in trace amount and large difference in its content is also detected for both plate and particle debris, oxidation wear mechanism is expelled and thus the abrasion action by hard oxide particles is the dominant mechanism [34].

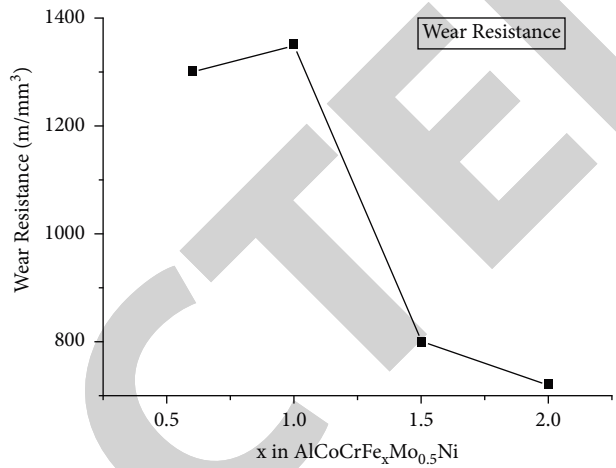

Figure 18: Wear resistance of $AlCoCrFexMo_{0.5}$ Ni alloys with respect to Fe content [32].

4.2. Effect of Boron. The $CuCoNiCrAl_{0.5}Fe$ with $x = 0$ to 1 has the FCC structure with boride precipitation and the boride vol. fraction is increased with boron content [27]. Consequently, the wear resistance of the alloy raised significantly with the inclusion of B as illustrated in Figure 20. The alloy with $x = 1$ named B-1.0 alloy has a greater resistance to wear even higher than that of SUJ2 wear-resistant steel.

Generally, the harder materials possess higher wear resistance. With the help of comparison (Figure 20), it can be identified that the B-0 and B-0.2 alloys exhibit wear resistance in the range of 316 and 17.4 stainless steels. The resistance to wear capability of B-0.6 alloy is very similar to that of cobalt-based superalloy (Stellite), which is attributed to the larger boride precipitates. Furthermore, the 736 HV harder B-1.0 alloys exhibit improved wear resistance than the SUJ2 bearing and SKD61 cold-work mould steels.

4.3. Effect of Vanadium. The graph shown in Figure 21 reveals that there is no significant change in the wear resistance of the $Al_{0.5}CoCrCuFeNiV_x$ HEA when vanadium content is not more than 0.6 and it is very comparable with the $Al_{0.5}CoCrCuFeNi$ [31]. But the wear resistance is increased significantly when the vanadium content reaches to 1.2 from 0.6. And a further increase in vanadium content from 1.2 to 2.0 does not make any significant change in the

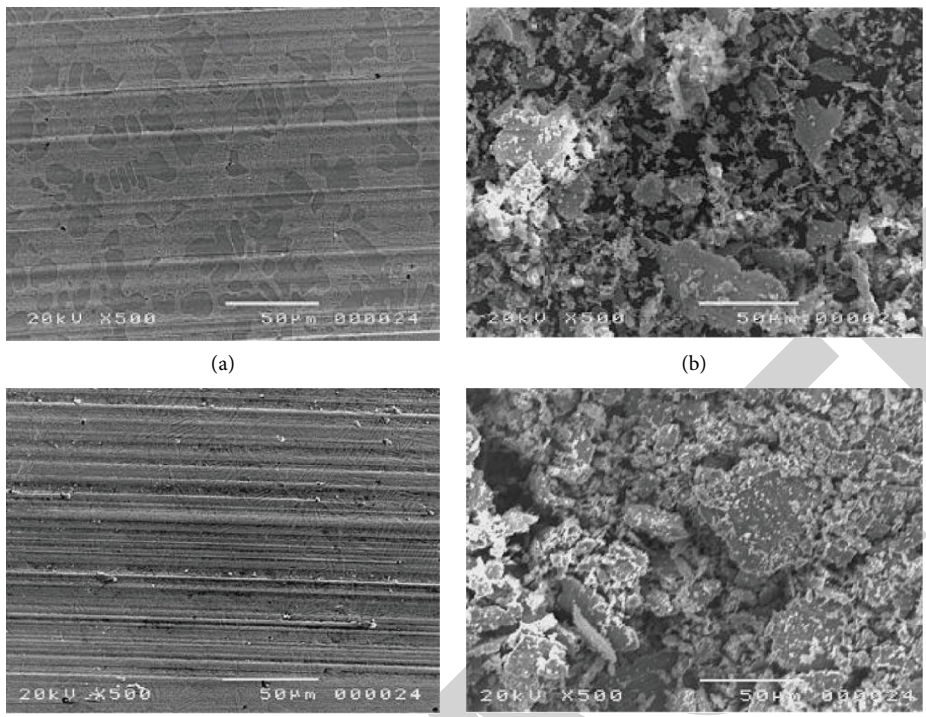

Figure 19: Worn surface and worn debris of AlCoCrFexMo0.5Ni alloys with different Fe contents: (a) $x = 0.6$, worn surface; (b) $x = 0.6$, worn debris; (c) X = 2.0, worn surface; (d) $x = 2.0$, worn debris [32].

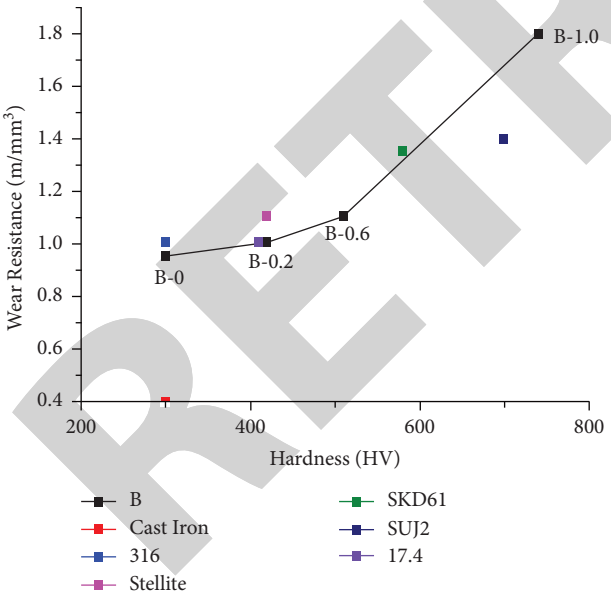

Figure 20: Wear resistance vs. hardness curve for CuCoNiCrAl$_{0.5}$Fe alloy with varying boron quantity [27].

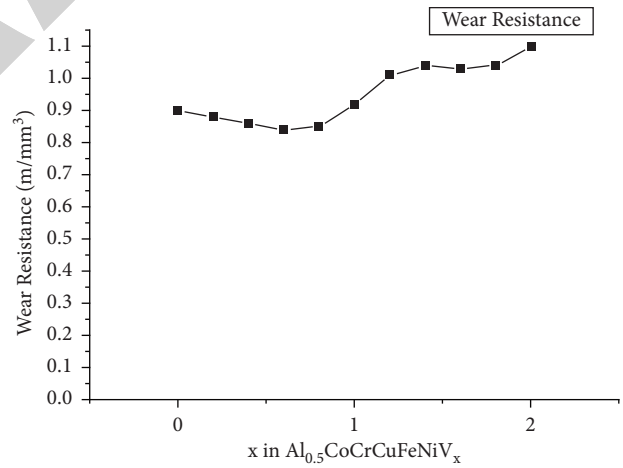

Figure 21: Wear resistance of $Al_{0.5}CoCrCuFeNiV_x$ HEA with different vanadium contents [31].

wear resistance of the alloy. Hence the $x = 1.0$ and 1.2 are said to be the optimum vanadium content for tool applications.

4.4. Effect of Aluminium and Titanium. Experimental results reveal that the resistance to wear property of $Al_{0.2}Co_{1.5}CrFeNi_{1.5}Ti$ and $Co_{1.5}CrFeNi_{1.5}Ti$ alloys is no less than twice superior to that of traditional steels with wear-resistant along with comparable microhardness [33]. From Figure 22 it can be easily identified that the harder $Al_{00}Ti_{10}$ and $Al_{02}Ti_{10}$ HEAs show off superior tribological behaviour when compared with soft $Al_{02}Ti_{05}$ and $Al_{00}Ti_{05}$ HEAs.

Figures 23(a)–23(c) illustrates the worn surface secondary electron images (SEI) of $Al_{02}Ti_{05}$ and $Al_{00}Ti_{05}$ samples. The worn-out surface of developed alloys demonstrates apparent features of plastic deformation and grooves and seem to be similar. Furthermore, it was found that except in darker regions in BEI (Figures 23(b)–23(d))

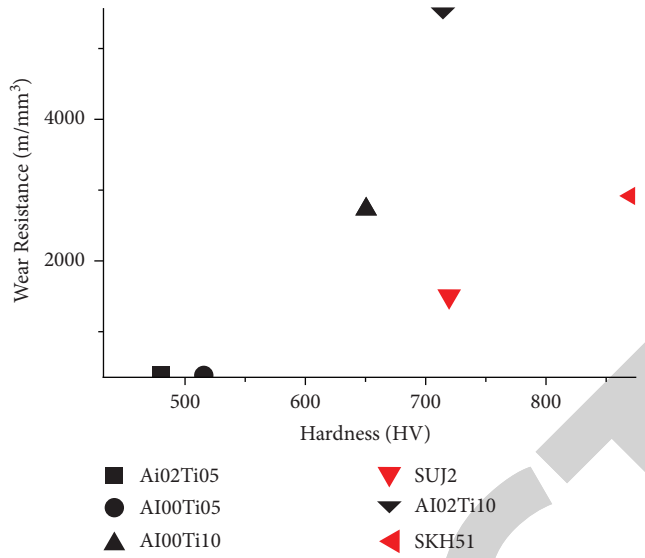

Figure 22: Variation in Adhesive wear behaviour and microhardness of various HEAs [33].

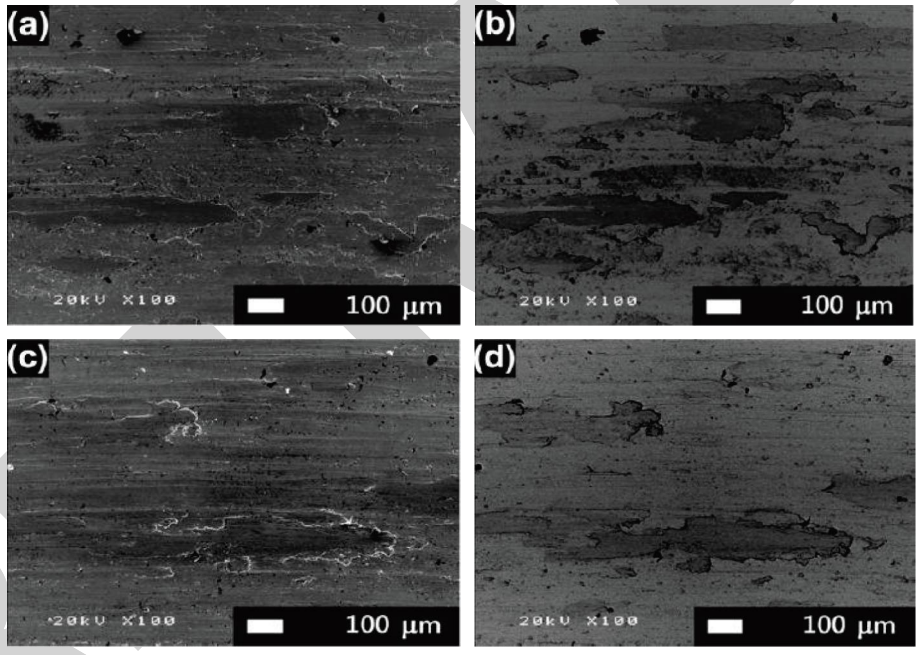

Figure 23: The worn-out surface morphology of $Al_{00}Ti_{05}$: (a) SEI and (b) BEI; $Al_{02}Ti_{05}$: (c) SEI and (d) BEI [33].

Table 3: Wear debris composition (in at. %) based on EDS analysis [33].

HEA	O	Fe	Cr	Ti	Ni	Co	Al
Al00Ti05	—	18.7	18.5	9.3	26.3	27.3	—
Al02Ti05	—	17.8	18.0	8.6	25.3	26.4	3.8
Al00Ti10	68.1	14.6	3.6	3.3	5.0	4.8	—
Al02Ti10	69.4	17.8	3.0	2.7	4.4	3.9	0.8

presence of oxygen is not found on the worn surface. The flake-like wear debris without oxygen content (Table 3) is obtained, so it is believed that the material is worn out from $Al_{02}Ti_{05}$ and $Al_{00}Ti_{05}$ devoid of several major oxidations.

The worn-out surface morphology of Al00Ti10 (Figure 24(a) and 24(b)) and Al02Ti10 (Figures 24(c) and 24(d)) shows only the signs of shallow scratches and few considerable features of oxidation which is in sharp disparity

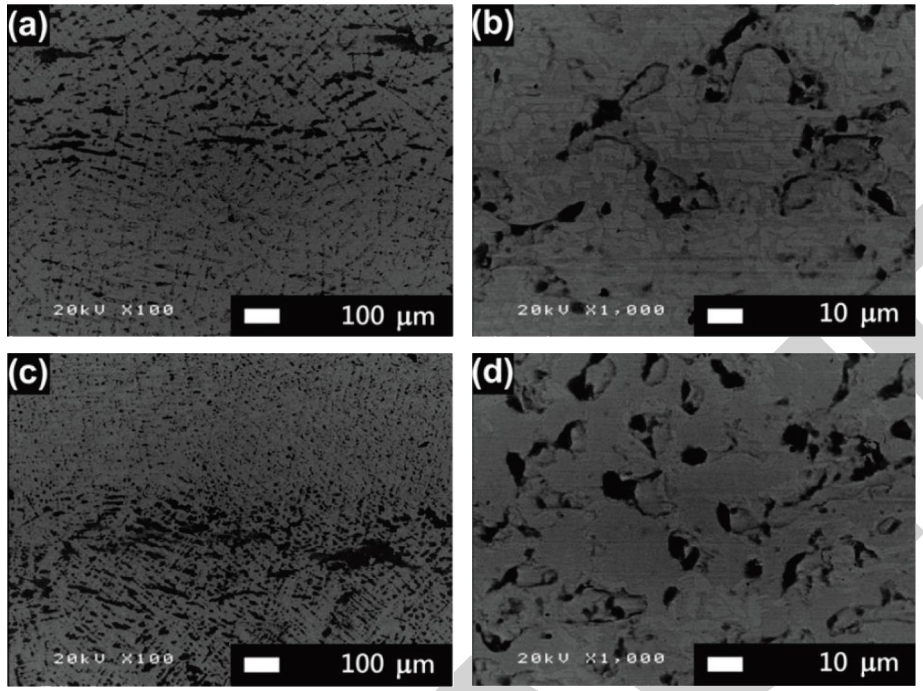

Figure 24: SEM BEI of worn-out morphology on Al00Ti10: (a) magnification 100X and (b) magnification 1000X; Al02Ti10: (c) magnification 100X and (d) magnification 1000X [33].

Table 4: Elementary Composition of dark areas in the worn surface of HEAs [33].

HEA	O	Al	Ti	Cr	Fe	Co	Ni
Al00Ti10 (at. %)	66.4	—	3.4	4.2	17.3	4.5	4.3
Al02Ti10 (at. %)	63.3	1.0	4.0	5.1	17.6	4.6	4.5

with the wear surface of Ti_{05} alloys. Furthermore, it is noteworthy that the dendrite–interdendrites structures of the alloy can still be recognised. Apparent signals of oxygen are found on EDS analysis on ID and DR regions with quite different compositions. The worn interdendritic composition is very similar to the alloys excluding the existence of O_2. Owing to a lower hardness of dendritic regions, they wear out severely with the black powder particles gathering in worn-out depressions. The attained EDS results depict that these black-coloured debris particles respective to Fe-rich oxides (Table 4) and the attained elementary composition are very much close to Ti10 alloy's debris particles. It is highly possible that these particles originated from worn-out debris of the SKH51 counter disk part since the worn-out debris and accrued black-coloured particles had a higher Fe concentration.

5. Applications

HEAs-based materials are set up as a wider structural and functional material with immense prospective for the choice in a broad array of various applications. Currently, the specific physical behaviour of HEAs, for example, $Al_{2.08}$CoCrFeNi, with persistent resistivity makes them successful materials for electronics-based applications. Hence extensive studies have to be made for these combinations of HEAs to improvise their future application. The superior tribological behaviour of B-1.0 alloy that is better than that of SUJ2-based wear-resistant steels depicts that the composition of $CuCoNiCrAl_{0.5}FeB_x$ based alloys showcase possible application in tool manufacturing, structural materials, both high temperature, and also in ambient room temperature condition.

6. Summary and Perspective

AlCoCrFeNi-based HEAs showcase attractive and unique properties for several applications in engineering components. This study involves the combination of several physical metallurgy aspects of HEAs with the composition of AlCoCrFeNi that includes various synthesis approaches, specific applications, and effects of alloying elements over its basic and functional characterisations such as mechanical, wear, and microstructural properties. The observations are depicted as enlisted below as follows:

(1) Various synthesis methods, such as arc melting, mechanical alloying, laser cladding, and plasma spraying are effectively adopted for developing HEAs with the composition of AlCoCrFeNi.

(2) These HEAs hold effective potential in an extensive assortment of applications, for instance, structural

and functional materials, particularly in nuclear reactors, turbine components, and also in various transport industries.

(3) Addition of alloying elements in AlCoCrFeNi HEAs depicts major variations and alters over the physical, mechanical, tribological, and microstructural properties

(4) AlCoCrFeNi-based HEAs possess ample wear property with respect to the addition of various alloying elements that includes Ti, B, and V. The Tribological property of AlCoCrCuFeNi and AlCoCrFeNiTi0.5 HEAs rubbing against 1Cr18Ni9Ti steel, ZrO_2 and SiC Ceramic in 90% H_2O_2 solution is better.

(5) The exceptional wear resistance of the HEAs is correlated to their thermal softening resistance and excellent antioxidation property. Hence it can be a potential candidate material as reinforcements in MMCs as a replacement for SiC-like ceramics.

Data Availability

Since it is a review article, the authors do not have any data associated with the article.

Conflicts of Interest

The authors declare that they have no conflicts of interest.

References

[1] J. W. Yeh, S. K. Chen, S. J. Lin et al., "Nanostructured high-entropy alloys with multiple principal elements: novel alloy design concepts and outcomes," *Advanced Engineering Materials*, vol. 6, no. 5, pp. 299–303, 2004.

[2] Y. F. Ye, Q. Wang, J. Lu, C. T. Liu, and Y. Yang, "Design of high entropy alloys: a single-parameter thermodynamic rule," *Scripta Materialia*, vol. 104, pp. 53–55, 2015.

[3] Y. Zhang, T. T. Zuo, Z. Tang et al., "Microstructures and properties of high-entropy alloys," *Progress in Materials Science*, vol. 61, pp. 1–93, 2014.

[4] B. Gludovatz, A. Hohenwarter, D. Catoor, E. H. Chang, E. P. George, and R. O. Ritchie, "A fracture-resistant high-entropy alloy for cryogenic applications," *Science*, vol. 345, no. 6201, pp. 1153–1158, 2014.

[5] M. A. Hemphill, T. Yuan, G. Y. Wang et al., "Fatigue behavior of Al0. 5CoCrCuFeNi high entropy alloys," *Acta Materialia*, vol. 60, no. 16, pp. 5723–5734, 2012.

[6] S. Q. Xia, X. Yang, T. F. Yang, S. Liu, and Y. Zhang, "Irradiation resistance in Al x CoCrFeNi high entropy alloys," *Journal of Occupational Medicine*, vol. 67, no. 10, pp. 2340–2344, 2015.

[7] Y. F. Ye, Q. Wang, J. Lu, C. T. Liu, and Y. Yang, "High-entropy alloy: challenges and prospects," *Materials Today*, vol. 19, no. 6, pp. 349–362, 2016.

[8] S. G. Ma and Y. Zhang, "Effect of Nb addition on the microstructure and properties of AlCoCrFeNi high-entropy alloy," *Materials Science and Engineering A*, vol. 532, pp. 480–486, 2012.

[9] S. Kapoor, R. Liu, X. J. Wu, and M. X. Yao, "TIMP-1 levels and their association with the development and progression of systemic malignancies," *The International Journal of Biological Markers*, vol. 28, no. 2, pp. 231–248, 2013.

[10] Y. Y. Chen, T. Duval, U. D. Hung, J. W. Yeh, and H. C. Shih, "Microstructure and electrochemical properties of high entropy alloys-a comparison with type-304 stainless steel," *Corrosion Science*, vol. 47, no. 9, pp. 2257–2279, 2005.

[11] K. K. Alaneme, M. O. Bodunrin, and S. R. Oke, "Processing, alloy composition and phase transition effect on the mechanical and corrosion properties of high entropy alloys: a review," *Journal of Materials Research and Technology*, vol. 5, no. 4, pp. 384–393, 2016.

[12] J. Chen, P. Niu, Y. Liu et al., "Effect of Zr content on microstructure and mechanical properties of AlCoCrFeNi high entropy alloy," *Materials & Design*, vol. 94, pp. 39–44, 2016.

[13] Y.-L. Chen, C.-W. Tsai, C.-C. Juan et al., "Amorphization of equimolar alloys with HCP elements during mechanical alloying," *Journal of Alloys and Compounds*, vol. 506, no. 1, pp. 210–215, 2010.

[14] C. Suryanarayana, "Mechanical alloying and milling," *Progress in Materials Science*, vol. 46, no. 1-2, pp. 1–184, 2001.

[15] A. W. Weeber, H. Bakker, H. J. M. Heijligers, and G. F. Bastin, "Compositional analysis of Ni-Zr powder during amorphization by mechanical alloying," *Europhysics Letters*, vol. 3, pp. 1261–1265, 1987.

[16] J. Chen, P. Niu, T. Wei et al., "Fabrication and mechanical properties of AlCoNiCrFe high-entropy alloy particle reinforced Cu matrix composites," *Journal of Alloys and Compounds*, vol. 649, pp. 630–634, 2015.

[17] W. Ji, Z. Fu, W. Wang et al., "Mechanical alloying synthesis and spark plasma sintering consolidation of CoCrFeNiAl high-entropy alloy," *Journal of Alloys and Compounds*, vol. 589, pp. 61–66, 2014.

[18] L. M. Wang, C. C. Chen, J. W. Yeh, and S. T. Ke, "The microstructure and strengthening mechanism of thermal spray coating NixCo0. 6Fe0. 2CrySizAlTi0. 2 high-entropy alloys," *Materials Chemistry and Physics*, vol. 126, no. 3, pp. 880–885, 2011.

[19] K. B. Zhang, Z. Y. Fu, J. Y. Zhang, W. M. Wang, S. W. Lee, and K. Niihara, "Characterization of nanocrystalline CoCrFeNiTiAl high-entropy solid solution processed by mechanical alloying," *Journal of Alloys and Compounds*, vol. 495, no. 1, pp. 33–38, 2010.

[20] M. Wang, "Composite coatings for implants and tissue engineering scaffolds," in *Biomedical Composites*, pp. 127–177, Woodhead Publishing, Sawston, Cambridge, 2010.

[21] A. S. M. Ang, C. C. Berndt, M. L. Sesso et al., "Plasma-sprayed high entropy alloys: microstructure and properties of AlCoCrFeNi and MnCoCrFeNi," *Metallurgical and Materials Transactions A*, vol. 46, no. 2, pp. 791–800, 2015.

[22] S. Zhang, C. L. Wu, J. Z. Yi, and C. H. Zhang, "Synthesis and characterization of FeCoCrAlCu high-entropy alloy coating by laser surface alloying," *Surface and Coatings Technology*, vol. 262, pp. 64–69, 2015.

[23] Q.-Y. Wang, R. Pei, S. Liu et al., "Microstructure and corrosion behavior of different clad zones in multi-track Ni-based laser-clad coating," *Surface and Coatings Technology*, vol. 402, Article ID 126310, 2020.

[24] Y. Shon, S. S. Joshi, S. Katakam, R. Shanker Rajamure, and N. B. Dahotre, "Laser additive synthesis of high entropy alloy coating on aluminum: corrosion behavior," *Materials Letters*, vol. 142, pp. 122–125, 2015.

[25] T. M. Yue and H. Zhang, "Laser cladding of FeCoNiCrAlCuxSi0· 5 high entropy alloys on AZ31 Mg alloy

substrates," *Materials Research Innovations*, vol. 18, no. sup2, pp. S2–S624, 2014.

[26] J. M. Zhu, H. M. Fu, H. F. Zhang, A. M. Wang, H. Li, and Z. Q. Hu, "Microstructures and compressive properties of multicomponent AlCoCrFeNiMox alloys," *Materials Science and Engineering A*, vol. 527, no. 26, pp. 6975–6979, 2010.

[27] C.-you Hsu, J.-W. Yeh, S.-K. Chen, and T.-T. Shun, "Wear resistance and high-temperature compression strength of Fcc CuCoNiCrAl0. 5Fe alloy with boron addition," *Metallurgical and Materials Transactions A*, vol. 35, no. 5, pp. 1465–1469, 2004.

[28] G. E. Wasielewski and R. A. Rapp, "The superalloys, vital high temperature gas turbine materials for aerospace and industrial power," pp. 287–316, John Wiley & Sons Inc, Hoboken, New Jersey, 1972.

[29] A. Inoue, "Stabilization of metallic supercooled liquid and bulk amorphous alloys," *Acta Materialia*, vol. 48, no. 1, pp. 279–306, 2000.

[30] X. Liu, W. Lei, L. Ma, J. Liu, J. Liu, and J. Cui, "On the microstructures, phase assemblages and properties of Al0. 5CoCrCuFeNiSix high-entropy alloys," *Journal of Alloys and Compounds*, vol. 630, pp. 151–157, 2015.

[31] M.-R. Chen, Su-J. Lin, J.-W. Yeh, M.-H. Chuang, S.-K. Chen, and Y.-S. Huang, "Effect of vanadium addition on the microstructure, hardness, and wear resistance of Al0. 5CoCrCuFeNi high-entropy alloy," *Metallurgical and Materials Transactions A*, vol. 37, no. 5, pp. 1363–1369, 2006.

[32] C.-Y. Hsu, T.-S. Sheu, J.-W. Yeh, and S.-K. Chen, "Effect of iron content on wear behavior of AlCoCrFexMo0. 5Ni high-entropy alloys," *Wear*, vol. 268, no. 5-6, pp. 653–659, 2010.

[33] M.-H. Chuang, M.-H. Tsai, W.-R. Wang, S.-J. Lin, and J.-W. Yeh, "Microstructure and wear behavior of AlxCo1. 5CrFeNi1. 5Tiy high-entropy alloys," *Acta Materialia*, vol. 59, no. 16, pp. 6308–6317, 2011.

[34] J.-M. Wu, S.-J. Lin, J.-W. Yeh, S.-K. Chen, Y.-S. Huang, and H.-C. Chen, "Adhesive wear behavior of AlxCoCrCuFeNi high-entropy alloys as a function of aluminum content," *Wear*, vol. 261, no. 5-6, pp. 513–519, 2006.